Check for updates

Systematic computer-aided disulfide design as a general strategy to stabilize prefusion class I fusion proteins

Karen J. Gonzalez[1,2], Kevin C. Yim[3], Jorge C. G. Blanco[3], Marina S. Boukhvalova[3] and Eva-Maria Strauch[1,2,4]*

[1]Institute of Bioinformatics, Franklin College of Arts and Sciences, University of Georgia, Athens, GA, United States, [2]Department of Medicine, School of Medicine, Washington University, St. Louis, MO, United States, [3]Sigmovir Biosystems, Inc., Rockville, MD, United States, [4]Department of Pharmaceutical and Biomedical Sciences, College of Pharmacy, University of Georgia, Athens, GA, United States

Numerous enveloped viruses, such as coronaviruses, influenza, and respiratory syncytial virus (RSV), utilize class I fusion proteins for cell entry. During this process, the proteins transition from a prefusion to a postfusion state, undergoing substantial and irreversible conformational changes. The prefusion conformation has repeatedly shown significant potential in vaccine development. However, the instability of this state poses challenges for its practical application in vaccines. While non-native disulfides have been effective in maintaining the prefusion structure, identifying stabilizing disulfide bonds remains an intricate task. Here, we present a general computational approach to systematically identify prefusion-stabilizing disulfides. Our method assesses the geometric constraints of disulfide bonds and introduces a ranking system to estimate their potential in stabilizing the prefusion conformation. We hypothesized that disulfides restricting the initial stages of the conformational switch could offer higher stability to the prefusion state than those preventing unfolding at a later stage. The implementation of our algorithm on the RSV F protein led to the discovery of prefusion-stabilizing disulfides that supported our hypothesis. Furthermore, the evaluation of our top design as a vaccine candidate in a cotton rat model demonstrated robust protection against RSV infection, highlighting the potential of our approach for vaccine development.

KEYWORDS

vaccine development, class I fusion proteins, prefusion stabilization, disulfide design, computational modeling

1 Introduction

Since the emergence of the severe acute respiratory syndrome coronavirus 2 (SARS-CoV-2) and the subsequent development of COVID-19 vaccines, it has become apparent that prefusion class I fusion proteins are potent vaccine candidates. This potential is not unique to SARS-CoV-2 and has also been illustrated in other pathogenic viruses, such as Hendra and Nipah (1, 2), parainfluenza virus types 1-4 (3), influenza (4), human metapneumovirus (hMPV) (5), and the respiratory syncytial virus (RSV) (6–8). Despite this, the intrinsic structural instability of these proteins poses a significant challenge when integrating them into vaccine formulations. As part of their function as membrane-fusion mediators, class I fusion proteins can irreversibly refold from their metastable prefusion state to a highly stable postfusion state (9). This spontaneous transition is a major hurdle in vaccine development, as potent neutralizing epitopes are often hidden in the protein's most stable structure, the postfusion state (10, 11). Consequently, stabilizing the prefusion conformation has been a continuous pursuit for maintaining the protein's immunogenicity and leveraging its potential as a vaccine component.

Understanding the conformational rearrangements of class I fusion proteins was largely possible thanks to the crystallization of the influenza virus hemagglutinin protein (12–14) and paramyxoviruses fusion proteins (15–18). As a common fusion mechanism, class I fusion proteins are initially matured by proteolytic cleavage, where a hydrophobic fusion peptide is left unconstrained to connect with the host cell (19, 20). Following its activation, the fusion-competent yet fragile prefusion state undergoes conformational changes, facilitating the fusion peptide's interaction with the target membrane (12, 21, 22). As this interaction progresses, the protein's C-terminus relocates, leading to the assembly of a highly stable six-helix bundle, the postfusion state. This structural transition ultimately enables the fusion of the viral and cellular membranes (23–25).

The structural analysis of the fusion mechanism has guided the prefusion stabilization of various class I fusion proteins by targeting regions prone to refolding (26). Historically, this goal has been achieved through an arduous manual exploration of the protein structure and extensive testing of protein mutants (1, 3, 26–31). We had previously pioneered a computational approach that significantly streamlined this demanding process, requiring only a few designs to identify stable prefusion versions (32). However, while our algorithm enabled the semi-automated introduction of stabilizing mutations using established molecular strategies, such as cavity filling, elimination of buried polar residues, and optimization of polar and electrostatic interactions, it did not allow for the incorporation of disulfide bonds.

To complement our original stabilization strategy, we have developed a general computational approach to systematically identify prefusion-stabilizing disulfides. Our method traces potential disulfides based on allowed distance and geometry, similar to other software (33–35). However, while correct geometry indicates the likelihood of bond formation, it may not directly correlate with stabilizing effects (33, 36). Consequently, we sought to tailor the disulfide design process to class I fusion proteins by

considering the conformational dynamics of the protein during the selection of prefusion-stabilizing bonds. We hypothesize that disulfides restricting the initial stages of the conformational switch are more impactful at increasing the stability of the prefusion state than those located on regions unfolding last. We applied our novel disulfide-design strategy to the RSV fusion (F) protein, as we had previously optimized a construct, the R-1b protein, using our first methodology (32). Consequently, we had an ideal test case to assess the cumulative enhancements offered by the integration of both our approaches. By combining our prior approach with this disulfide-design strategy, we have successfully increased the stability of the RSV F protein without compromising its immunogenic properties.
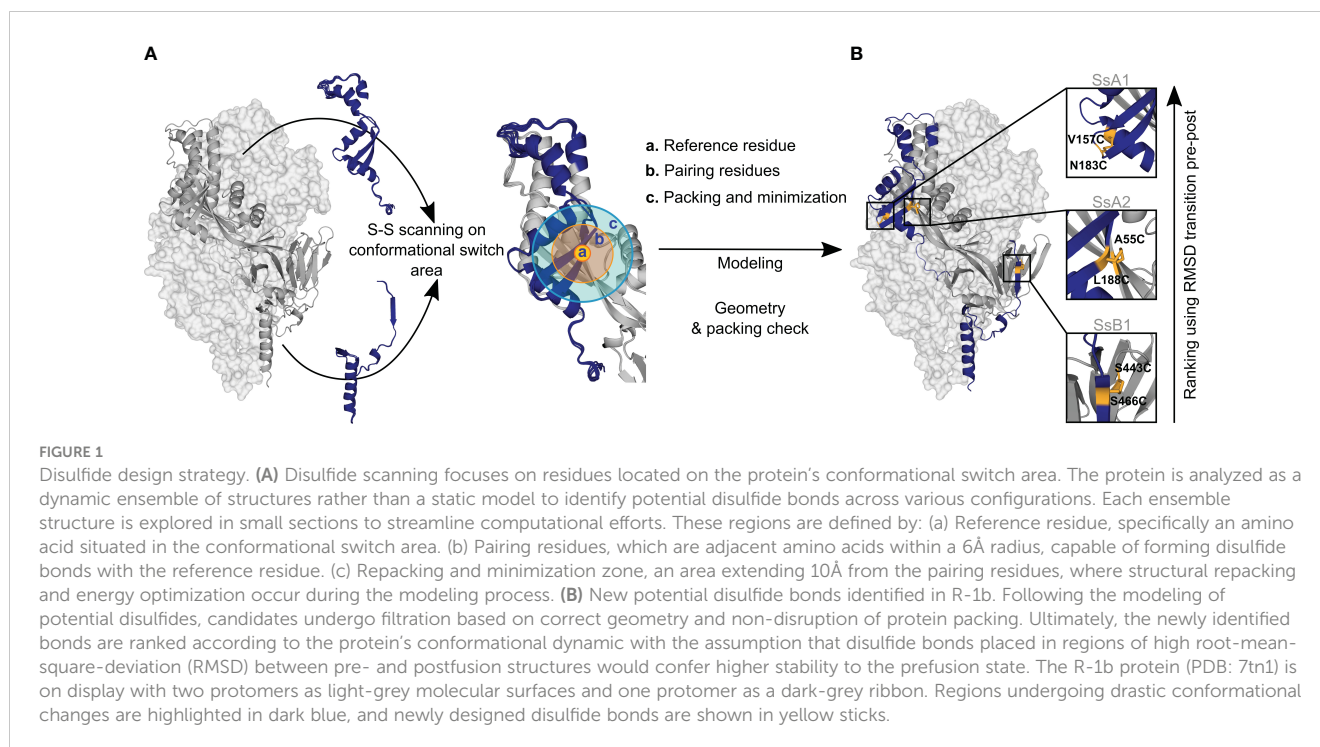
2 Results

2.1 Disulfide bond design strategy

Inspired by the efficacy of non-native disulfides in stabilizing the prefusion conformation of class I fusion proteins (1, 3, 7, 29), we have developed a computational approach to identify these covalent bonds. Building upon a previously proposed concept (5), our computational strategy is centered on identifying novel disulfides within regions undergoing significant relocation during the prefusion-to-postfusion transition (Figure 1A). Using PyRosetta as the disulfide scanning tool (37, 38), we first identify potential disulfide bonds via the proximity of Cβ atoms. However, recognizing that proteins are inherently dynamic and that resolved structures represent only single instances in time, we perform this analysis across a spectrum of potential conformations derived from structural energy minimization (39–41). This relaxation process is guided by electron density data to prevent the introduction of artifacts due to excessive deviations from the protein's original configuration.

In each conformation of the protein ensemble, residues within a 6Å radius are mutated to cysteine and disulfide bonds are enforced during a focused round of energy minimization and protein repacking (Figure 1A). With this focused structural sampling, we not only mitigate computational load but also ensure that the newly introduced disulfide aligns with the specific protein conformation under study. Finally, to increase the probability of successful disulfide formation, we apply a filtering process, assessing potential bonds for Rosetta disulfide energy (dslf_fa13) (42, 43) and geometric adequacy (Figure 2A) while ensuring the protein packing is not disrupted.

To evaluate the extent to which disulfide design could complement and enhance our existing computational framework, we applied our methodology to our previously optimized variant of the RSV F, the R-1b protein (32). This implementation led to the identification of 8 potential intrachain disulfides within regions involved in the protein's conformational switch. Notably, one of these disulfides corresponded to the most effective non-native disulfide previously reported for RSV F, the S155C-S290C disulfide (7) (Figure 2A).

With the goal of identifying metrics that could rank disulfides based on their potential stabilizing effects, we analyzed the geometric constraints of disulfides with prior experimental data

FIGURE 1
Disulfide design strategy. **(A)** Disulfide scanning focuses on residues located on the protein's conformational switch area. The protein is analyzed as a dynamic ensemble of structures rather than a static model to identify potential disulfide bonds across various configurations. Each ensemble structure is explored in small sections to streamline computational efforts. These regions are defined by: (a) Reference residue, specifically an amino acid situated in the conformational switch area. (b) Pairing residues, which are adjacent amino acids within a 6Å radius, capable of forming disulfide bonds with the reference residue. (c) Repacking and minimization zone, an area extending 10Å from the pairing residues, where structural repacking and energy optimization occur during the modeling process. **(B)** New potential disulfide bonds identified in R-1b. Following the modeling of potential disulfides, candidates undergo filtration based on correct geometry and non-disruption of protein packing. Ultimately, the newly identified bonds are ranked according to the protein's conformational dynamic with the assumption that disulfide bonds placed in regions of high root-mean-square-deviation (RMSD) between pre- and postfusion structures would confer higher stability to the prefusion state. The R-1b protein (PDB: 7tn1) is on display with two protomers as light-grey molecular surfaces and one protomer as a dark-grey ribbon. Regions undergoing drastic conformational changes are highlighted in dark blue, and newly designed disulfide bonds are shown in yellow sticks.

(7, 26, 44). Interestingly, we observed that a significant number of these previously tested disulfides exhibited appropriate geometric configurations yet failed to enhance protein stability. This observation suggested that other factors beyond geometric parameters might play a role in determining the stabilizing capabilities of disulfide bonds. Consequently, we sought to complement our geometry analysis by exploring the role of the protein's dynamics in identifying prefusion-stabilizing disulfides. We hypothesized that substitutions restricting the initial conformational changes of the protein would have a stronger impact on the stability of the prefusion state than those preventing the final stages of the rearrangement.
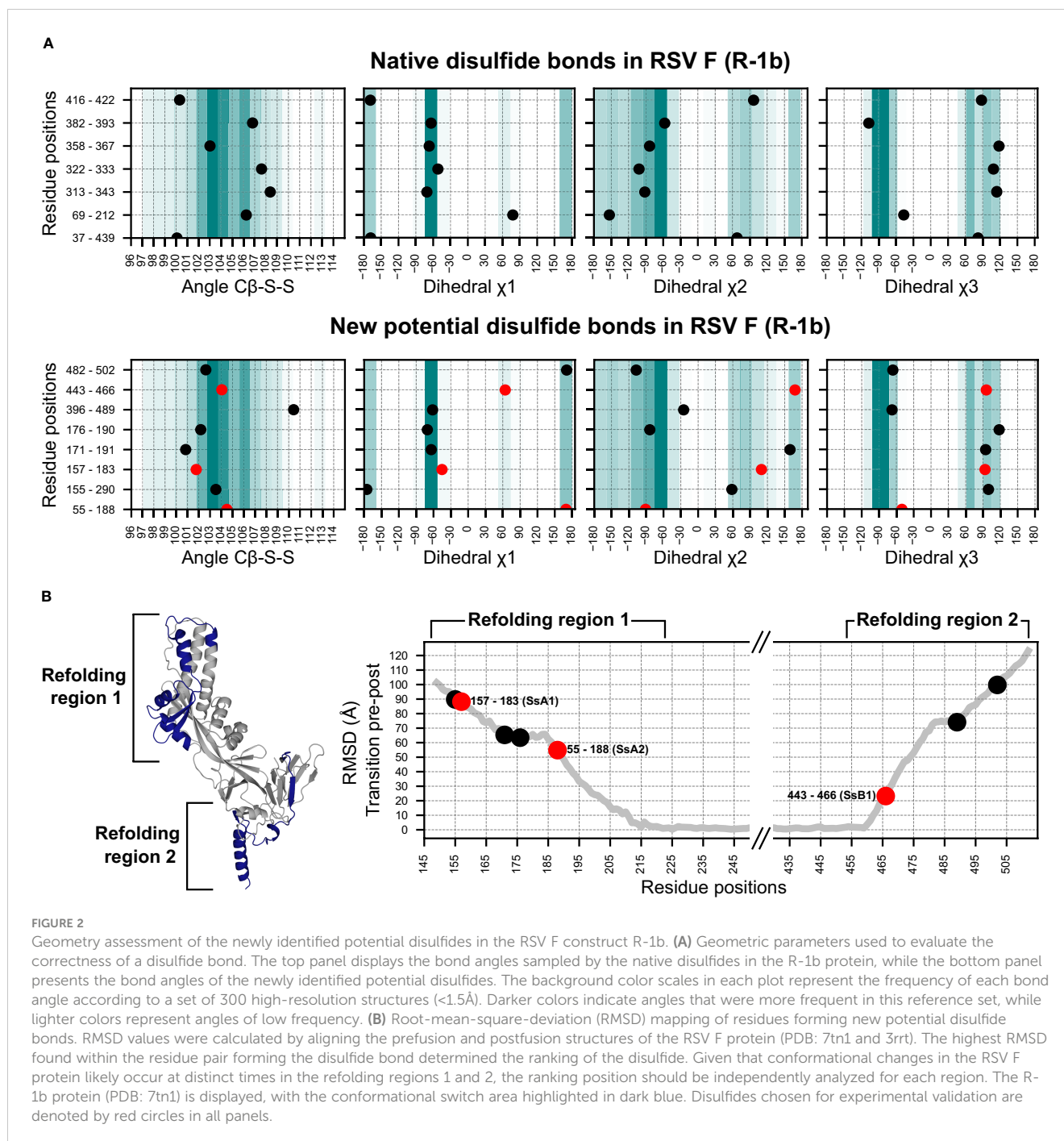
To integrate this concept into our selection process, we assumed that regions displaying higher root-mean-square-deviation (RMSD), when comparing the prefusion and postfusion structures, are more likely to unfold at an earlier stage. As a result, RMSD served as the quantitative metric to rank disulfide candidates according to their potential for prefusion stabilization (Figure 2B). Importantly, given that conformational changes in the refolding region 1 (protein head) likely trigger conformational changes in the refolding region 2 (membrane-proximal domain) (30), our ranking system was applied independently to each refolding region.

We expressed three distinct disulfide variants to validate our design and ranking approaches, each exhibiting well-differentiated RMSD values (Figure 2B). The selected disulfides included *V157C-N183C* (design SsA1), located at the beginning of the refolding region 1, *A55C-L188C* (design SsA2), found at the middle of the refolding region 1, and *S443C-S466C* (design SsB1), situated at the beginning of the refolding region 2 (Figures 1B, 2B). Notably, while this manuscript was in preparation, an independent study published experimental validations for the latter two disulfides (45).

2.2 Biochemical characterization of disulfide candidates

All three designs, SsA1, SsA2, and SsB1, were successfully expressed and purified as trimeric proteins, as confirmed by size exclusion chromatography (SEC) (Figure 3A). Additionally, the expression yield of these variants showed no significant changes when compared to the parent construct R-1b (Figure 3A). As anticipated, the designed proteins exhibited notable improvements in thermal stability compared to R-1b, with melting temperature increments of 2.5°C (SsB1), 5.5°C (SsA2), or 12.5°C (SsA1) (Figure 3B). This enhancement in heat stability aligned well with our proposed hypothesis, emphasizing that disulfides restricting the initial stages of protein unfolding can have a more profound impact on the overall stability of the prefusion conformation. Remarkably, the thermal stability of design SsA1 surpassed that of the current RSV vaccine DS-Cav1 (7) by approximately 6.5°C (Figure 3B). However, it is important to note that these results do not imply that the V157C-N183C disulfide in SsA1 is inherently superior to the S155C-S290C disulfide found in DS-Cav1. Instead, the evident improvement observed in SsA1 likely arises from a synergistic effect resulting from introducing the new disulfide and the preexisting mutations in R-1b (32).

The melting curve of SsA1 and DS-Cav1 presented two possible unfolding stages, characterized by a low-intensity peak at approximately 55°C and a high-intensity peak above 65°C (Figure 3B). To assess the structural significance of these unfolding phases, we conducted binding assays with prefusion-specific antibodies after subjecting the proteins to heat treatment. Our results revealed that SsA1 effectively preserves the prefusion conformation at high temperatures, as evidenced by its strong binding to D25 (46, 47), hRSV90 (48), and MPE8 (49) even after

FIGURE 2
Geometry assessment of the newly identified potential disulfides in the RSV F construct R-1b. **(A)** Geometric parameters used to evaluate the correctness of a disulfide bond. The top panel displays the bond angles sampled by the native disulfides in the R-1b protein, while the bottom panel presents the bond angles of the newly identified potential disulfides. The background color scales in each plot represent the frequency of each bond angle according to a set of 300 high-resolution structures (<1.5Å). Darker colors indicate angles that were more frequent in this reference set, while lighter colors represent angles of low frequency. **(B)** Root-mean-square-deviation (RMSD) mapping of residues forming new potential disulfide bonds. RMSD values were calculated by aligning the prefusion and postfusion structures of the RSV F protein (PDB: 7tn1 and 3rrt). The highest RMSD found within the residue pair forming the disulfide bond determined the ranking of the disulfide. Given that conformational changes in the RSV F protein likely occur at distinct times in the refolding regions 1 and 2, the ranking position should be independently analyzed for each region. The R-1b protein (PDB: 7tn1) is displayed, with the conformational switch area highlighted in dark blue. Disulfides chosen for experimental validation are denoted by red circles in all panels.

heating at 65°C, and continued binding to D25 and hRSV90 even after heating at 70°C (Figure 3C). In contrast, although DS-Cav1 retained binding to D25 and hRSV90 at 65°C, the reduced binding to MPE8 indicated the loss of the protein's quaternary structure at this temperature (Figure 3C). These results not only confirmed the increased stability of SsA1 compared to DS-Cav1 but also demonstrated that the apparent unfolding observed at ~55°C has no substantial impact on the conformation of prefusion antigenic regions. Instead, it is the second melting peak that determines the protein's complete unfolding. It is worth noting that these two unfolding phases are evident in all tested constructs except SsB1. Given that SsB1 is the only variant designed to prevent

conformational changes at the refolding region 2, it is likely that the peak around 55°C seen in the other proteins results from partial unfolding of this membrane-proximal region.

Although our antibody binding assays also reveal a diminished interaction between SsA1 and the quaternary antibody AM14 (47, 50) (Figure 3C), this result might stem from the disruption of the AM14 epitope rather than dissociation of the trimeric state. Previous studies with monoclonal antibody-resistant mutants (MARMs) have identified the N183K mutation as an AM14-escape variant (50). Therefore, given that our SsA1 design includes a substitution at position 183 (N183C), it is possible that this mutation is interfering with AM14 binding.
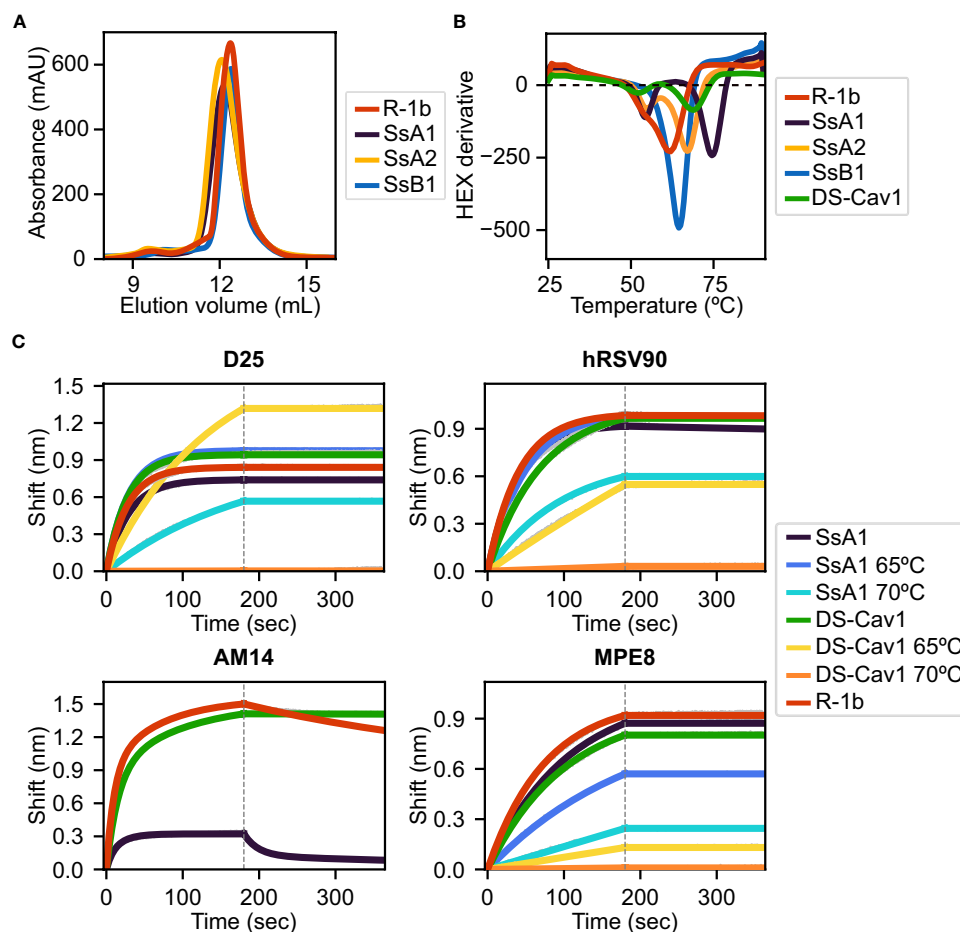
FIGURE 3
Biochemical characterization of R-1b variants containing designed non-native disulfide bonds. **(A)** Size-exclusion chromatography. **(B)** Differential scanning fluorimetry of designed variants in comparison with the clinical candidate DS-Cav1 (7). On display are shown averaged values over three replicates. Estimated melting temperatures are R-1b 62°C, SsA1 74.5°C, SsA2 67.5°C, SsB1 64.5°C, and DS-Cav1 68°C. **(C)** Binding of variants SsA1, R-1b, and DS-Cav1 to prefusion antibodies after heat treatment. R-1b was only tested at room temperature as the protein's melting temperature was below the set temperature for the assays. Plotted values correspond to binding at the highest protein concentration (200nM). Binding data are shown in grey, while the best fits to a 1:1 binding model (D25, hRSV90, and MPE8), or a 2:1 binding model (AM14) are shown in distinct colors. The end of the association time is delimited with a dotted line. Binding constants are shown in Supplementary Table 1.

The physical stability of the SsA1 protein was further tested under various storage conditions, including one week at 25°C, one month at 5°C and -20°C, and over one year at -80°C. Antibody binding assays with prefusion-specific antibodies demonstrated that both the SsA1 design and its parent construct, as well as DS-Cav1, effectively preserved the prefusion state under all tested conditions (Supplementary Figure 1).

2.3 Disulfide bond detection in SsA1

To verify the successful formation of the V157C-N183C disulfide bond in design SsA1, we conducted a tandem liquid chromatography mass spectrometry (LC-MS/MS) analysis. To achieve this, the protein underwent two consecutive alkylation reactions, enabling the differentiation of free cysteines from those involved in disulfide bonding. In the first alkylation step, we used iodoacetic acid (IAA) to attach carboxymethyl groups specifically

on free cysteines. Subsequently, a second alkylation reaction was carried out with iodoacetamide (IAM) to introduce carbamidomethyl groups on disulfide-bonding cysteines, following the reduction of the disulfide bond. Finally, peptide fragments obtained from trypsin digestion were subjected to LC-MS/MS analysis.

The ion chromatograms of peptides containing cysteines 157 (**C**LHLEGEVNK) and 183 (AVVSLS**C**GVSVLTSK) displayed two distinct retention times, indicating the presence of both carboxymethyl and carbamidomethyl in the peptides (Supplementary Figure 2). Although this signified that the cysteines 157 and 183 existed in both free and bound states, the predominance of disulfide-bonding cysteines was evident in base peak intensity of the samples' mass spectrum (Supplementary Figure 2). Specifically, the normalization level (NL) value of each peak indicated that the relative concentration of the peptide **C**LHLEGEVNK in the disulfide-bonding state was ~29 times higher than in the unbound state. Similarly, the concentration of the peptide AVVSLS**C**GVSVLTSK in

the disulfide-bonding state was ~15 times higher than in the unbound state. The fragmentation spectrum of both peptides, confirming the disulfide formation (carbamidomethyl labeling), is shown in Supplementary Figures 3, 4.

2.4 Immunogenicity of SsA1 in cotton rats

The SsA1 protein was selected for a vaccination study to investigate the potential effects of enhanced prefusion-stability on the immunogenicity of R-1b. Cotton rats were immunized intramuscularly with 10 or 100 μg of AddaSO3-adjuvanted R-1b or SsA1 at weeks 0 and 4 (Figure 4A). Three weeks after the booster immunization, sera were collected to examine the IgG response against prefusion and postfusion RSV F proteins, along with their neutralizing activity (Figure 4A). Notably, animals immunized with either R-1b or SsA1 presented a robust RSV F prefusion-specific response, showing equivalent antibody titers against RSV A or RSV B F proteins, as measured by ELISA (Figures 4B, D). Similarly, no significant differences were observed regarding RSV A2 F postfusion-specific antibodies, although SsA1 vaccination evidenced slightly lower titers (Figure 4C). Finally, both immunogens induced comparable levels of antibody neutralizing titers, with most doses surpassing the neutralizing titers generated by natural RSV A2 infection (Figure 4E).

Our vaccination study concluded with an RSV A2 challenge to assess the efficacy and safety of our proteins as potential vaccine candidates. Overall, animals vaccinated with either R-1b or SsA1 successfully cleared the virus from the lung and nose (Figure 4F) and did not exhibit vaccine-enhanced disease, as evidenced by low levels of interleukin (IL) 4, IL-13, and interferon-gamma (IFN-g) (Figures 4G–I). Vaccine safety was further supported by the absence of enhanced pulmonary histopathology. Animals vaccinated with 10 μg of R-1b or SsA1 presented minimal lung lesions, which did not exceed those observed in animals mock-immunized with PBS, while no histopathology was detected in animals immunized with 100 μg doses (Supplementary Figure 5). Collectively, likely due to the high dosage used, our vaccination data could not reveal differences in RSV protection based on the physical stability of the immunogen. However, it remains unclear whether the disruption of the AM14 binding site could hinder any potential improvement.

2.5 Epitope-specific antibody response

To gain further insights into the epitope-specific response elicited by SsA1 and R-1b, we conducted antibody binding competition assays against D25, hRSV90, MPE8, and 131-2A (54). This competition was carried out following the interaction of the R-1b antigen with different concentrations of pooled serum three weeks post-boost vaccination. Consistent with our ELISA findings, the sera from SsA1 or R-1b vaccinated animals exhibited strong competition for binding sites specific to the prefusion state (Figure 5). Notably, vaccinations with SsA1 demonstrated a higher prevalence of antibodies targeting the antigenic sites Ø and V. In

contrast, antibodies specific to the postfusion state were predominantly observed in animals vaccinated with R-1b, while quaternary antibodies were equally abundant in both vaccination groups (Figure 5). Altogether, our results suggest that even though the overall protection against RSV seems comparable with both immunogens, there are variations in the specificity of the antibody response originating from the differences in the physical stability of their respective binding sites. Consequently, it is likely that more pronounced differences in protection may become apparent at reduced vaccination dosages.

3 Discussion

Given the clinical significance of prefusion class I fusion proteins (55–58) and the proven effectiveness of non-native disulfides in enhancing protein stability (1, 3, 7, 29), we have developed a computational approach to identify prefusion-stabilizing disulfide bonds. While we had previously pioneered a semi-automated method aimed at increasing the stability of class I fusion proteins, we recognized the need to complement it due to its primary emphasis on optimizing non-covalent interactions. Indeed, our prefusion-stabilized RSV F protein, R-1b, emerged as an ideal candidate for exploring the influence of designed disulfide bonds, as its optimization was exclusively centered on reinforcing weak molecular forces (32). Notably, despite the extensive research on stabilizing the prefusion RSV F (7, 26, 30, 44, 45), our disulfide search has uncovered previously unexplored mutations. These findings highlight the comprehensive analysis that computational design offers, showcasing its potential benefits not only for novel optimizations but also for the enhancement of established vaccine candidates.

During the preparation of this manuscript, an independent study was published, assessing the impact of various mutations on the stability of the prefusion RSV F protein, including the introduction of new disulfide bonds (45). While some of our findings aligned, such as the identification of the A55C-L188C and S443C-S466C disulfides, with the former proving more stabilizing than the latter, other results were exclusive to each study. Of note, this independent investigation reported a newly discovered highly stabilizing disulfide, namely T103C-I148C. We noticed that this disulfide was overlooked with our approach due to its location in the fusion peptide region, which we had occluded. Our methodology, which initiates the scanning process by comparing prefusion and postfusion conformations, excluded the fusion peptide region because of its absence in the postfusion conformation. However, upon revisiting our scanning process, this time including the fusion peptide, the T103C-I148C disulfide was successfully identified (Supplementary Figure 6).

Unlike other computational methods that begin disulfide prediction from a single protein conformation (33–35), our approach evaluates an ensemble of conformations derived from structural energy minimization. Since proteins are dynamic and crystal structures represent only one possible state, potential disulfides can be easily overlooked when the crystallized state fails to meet initial filtering criteria. For instance, slight shifts in loops
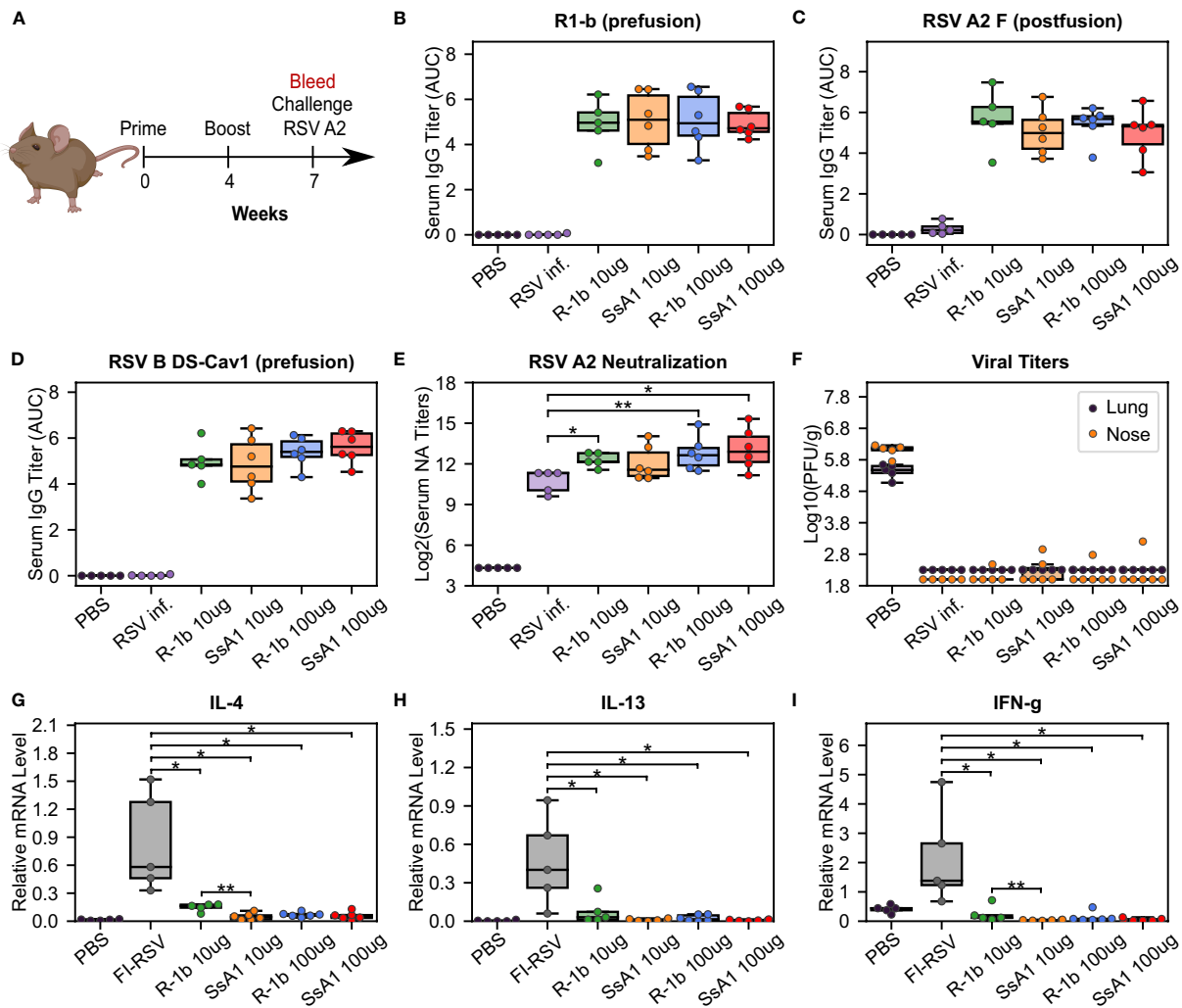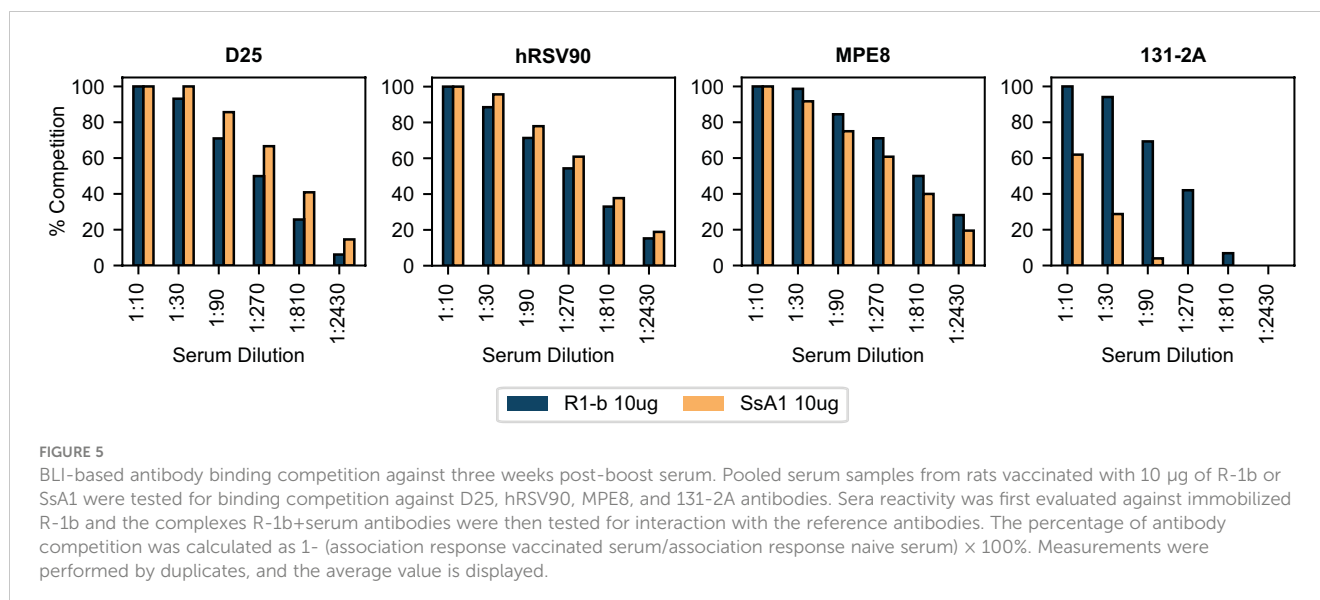
FIGURE 4

Immunogenicity and vaccine-enhanced disease assessment of R1-b variants in cotton rats. **(A)** Vaccination study regimen. **(B)** Serum IgG binding against R1-b, **(C)** RSV A/A2 F (postfusion) (51), and **(D)** RSV B/18537 DS-Cav1 (52) proteins measured by ELISA three weeks post-boost. Control experiments corresponded to a mock vaccination with PBS and a primary infection with RSV A/A2 on day 0 (RSV inf.). Serum titers were estimated with GraphPad Prism 9.0 (53) (53) using the area under the curve (AUC) measurement with a baseline of 0.3 absorbance units and $\log_3$-transformed serum dilutions. Sera were serially diluted three-fold from 1:60,000 (R1-b binding) or 1:20,000 to a total of 7 dilutions. **(E)** Serum neutralizing (NA) titers against RSV A/A2 using sera three weeks post-boost. **(F)** RSV A/A2 viral titers in lung and nose five days after challenge. Viral titers were determined by plaque-forming units (PFU) per gram of tissue. **(G)** Vaccine-enhanced disease assessment according to mRNA levels of Interleukin-4 (IL-4), **(H)** Interleukin-13 (IL-13), and **(I)** Interferon gamma (IFN-g). mRNA levels were measured in lung tissue five days post-challenge. A mock vaccination with PBS was used as the negative control, and cotton rats immunized with formalin-inactivated RSV (FI-RSV) were used as the positive control. The relative expression units were normalized to the level of β-actin mRNA ("housekeeping gene") expressed in the corresponding sample. In all panels, each animal is represented by a circle corresponding to the average value from two measurements. The distribution of the data is shown in boxplots. All boxplots show the median as a central line, lower and upper quartiles as the box limits, and minimum to maximum values as whiskers. Pairwise statistical analyses were performed with a two-tailed T-test for the ELISA experiments and the vaccine-enhanced disease assessment. A Mann-Whitney U test was used for the neutralization data. *, $p \leq 0.05$; **, $p \leq 0.01$. The cotton rat cartoon was created with BioRender through licensing with the Institute of Bioinformatics at the University of Georgia.

might miss the Cβ-Cβ distance threshold, or the disulfide geometry may not fit the crystallized conformation. For the non-native disulfides found in this study and those identified by our methodology but experimentally validated elsewhere [155-290 (7) and 103-148 (45)], we observed that despite Cβ-Cβ distances varying by less than 1Å across different structures (Supplementary Figure 7A), only specific conformations could accommodate the geometric constraints determining the potential for disulfide formation (Supplementary Figure 7B). This was evident with our SsA2 design and the highly stabilizing T103C-I148C disulfide.

Although the crystallized structures did not satisfy the Rosetta disulfide energy (dslf_fa13) and rotation/translation distance requirements, and most relaxed structures also failed to meet these parameters, a few conformational variants successfully accommodated these disulfides, enabling their discovery. Consequently, analyzing conformational ensembles may facilitate a more comprehensive search for potential disulfide bonds.

While predicting the likelihood of disulfide formation is feasible through analyzing the bond's geometry (33–35), a metric to rank the stabilizing effect of a designed disulfide is not currently available.

FIGURE 5

BLI-based antibody binding competition against three weeks post-boost serum. Pooled serum samples from rats vaccinated with 10 µg of R-1b or SsA1 were tested for binding competition against D25, hRSV90, MPE8, and 131-2A antibodies. Sera reactivity was first evaluated against immobilized R-1b and the complexes R-1b+serum antibodies were then tested for interaction with the reference antibodies. The percentage of antibody competition was calculated as 1- (association response vaccinated serum/association response naive serum) × 100%. Measurements were performed by duplicates, and the average value is displayed.

Some studies have proposed using residue B-factors to select stabilizing disulfides, recognizing that rigidifying highly flexible areas can enhance protein stability (33, 36). However, this metric may not fully capture the complexities of the prefusion state in class I fusion proteins. The RSV F protein serves as a clear example. Depending on the crystallization method and quality, the RSV F region with the highest B-factors can vary between the head and the membrane-proximal domains, as evident in the PDBs 5c69 and 5w23 (30, 59), respectively. Interestingly, despite this variability, one of the most stabilizing disulfides reported for RSV F, the S155C-S290C disulfide (7), falls in a region of relatively low B-factor. This observation underscores the challenges of predicting disulfide-induced stabilization of the prefusion conformation and emphasizes the need to consider other factors when estimating the potential success of an engineered disulfide bond.

As class I fusion proteins undergo intricate refolding processes, we explored whether the dynamics of their conformational changes could provide insight into the ability of a non-native disulfide to stabilize the prefusion conformation. To investigate this, we employed the RMSD of the prefusion-to-postfusion transition as a quantitative metric for monitoring conformational dynamics. We hypothesize that regions with high RMSD are more prone to unfolding first during the transition to the postfusion state, and inhibiting these initial rearrangements is more effective at stabilizing the prefusion conformation. Our results support this hypothesis, revealing poorer thermal stability in disulfides located in regions of smaller RMSD values. However, since conformational changes in the RSV F protein probably initiate in the refolding region 1 followed by the refolding region 2 (30), further studies are essential to clarify whether the overall RMSD value can inform the stabilizing properties of a disulfide bond or if its utilization requires subdivision based on refolding regions.

For the RSV F protein, we have found that disulfides placed in proximity to the fusion peptide have a greater effect on the stability of the prefusion state than those located nearer to the membrane-proximal region. Interestingly, within the refolding region 1,

increases in melting temperature aligned with the positioning of the designed disulfides, with bonds closer to the N-terminus of the F1 subunit providing higher thermal stability (Figure 3B). These results might reflect the dynamics of the protein, suggesting that disulfide bonds restricting the initial stages of the conformational switch have a more significant impact on the stability of the prefusion state than those hindering the unfolding at later stages. However, since the precise sequence of events preceding the translocation of the fusion peptide has not been definitively determined, it is still unclear whether the release of the fusion peptide promotes the refolding of the heptad repeat A region or if conformational changes at the apex initiate the projection of the fusion peptide (30). Different fusion inhibition studies seem to support the former hypothesis, showing that small molecules tethering the fusion peptide to the heptad repeat B region can effectively prevent triggering to the postfusion state (60–62). Our findings appear to align with this fusion model as well. If conformational shifts were to initiate at the apex and propagate downstream, our A55C-L188C disulfide, located closer to the apex, should have exhibited the most significant stabilizing effect by hindering the initial unfolding phase. Contrarily, it was the V157C-N183C disulfide, situated closer to the fusion peptide, which displayed the most pronounced stabilizing impact. Therefore, it is likely that the release of the fusion peptide drives the subsequent conformational changes and its inhibition results in a more pronounced stabilization of the prefusion state, as has been seen in other viral families (63).

A common strategy for designing prefusion-stabilizing disulfides in class I fusion proteins involves linking the conformational switch area to regions that remain unchanged during the pre- to postfusion transition (5, 7, 28, 45). This approach is believed to be more effective at maintaining the prefusion structure, as partial refolding can still occur when the disulfide bond only connects regions prone to change. In our study, we did not focus on this aspect since our starting construct had previously been optimized to preserve the prefusion conformation.

However, this is an important consideration when working with wild-type sequences. While the success of tethering a mobile region to a fixed region is well-documented, there are also reports of effective disulfides within the refolding area, particularly when they are located near the fusion peptide (63). Therefore, preventing the very beginning of the conformational change may be beneficial regardless of the connected areas, but partial refolding may become more influential as the bond is positioned further away from the fusion peptide or the starting refolding point. In such cases, linking the flexible region to a stable region may be more successful at maintaining a proper folding.

At this point, a clear correlation between the stability of the prefusion state and its immunogenic properties remains to be established, which could be examined by reducing the overall dosage. It is possible that the disruption of the AM14 binding site in SsA1 impeded its potential for enhanced immunogenicity (45). Prior studies aiming to improve DS-Cav1 stability have shown a relationship between physical stability and increased RSV protection, particularly when employing interprotomer disulfides to ensure an appropriate quaternary structure (26). However, this association is not consistently observed, as other studies incorporating interprotomer disulfides and increased stability have not reported a corresponding increase in immunogenicity (44, 64). Our observations from previously reported studies (26, 44, 45, 64) indicate that disulfides involved in enhanced immunogenicity primarily stabilize antigenic regions. Hence, it is probable that the local stability of antigenic regions might be the determining factor in increasing immunogenicity rather than the overall protein stability. Within our study, we did notice that antibodies targeting the antigenic site Ø, which was stabilized by the disulfide V157C-N183C, were slightly higher in vaccinations with SsA1 (Figure 5). However, this effect could also be attributed to the disruption of the AM14 binding site and a potential reduction in interclonal competition. Nevertheless, despite the complexities surrounding the relationship between stability and immunogenicity, strategic placement of disulfide bonds may offer opportunities to enhance the quality of the antibody response.

4 Materials and methods

4.1 Computational approach to design disulfide bonds

All computational analyses were performed with the Rosetta version: 2020.10.post.dev+12.master.c7b9c3e c7b9c3e4aeb1febab211d63da2914b119622e69b

4.1.1 Definition of conformational switch area

To ensure the RSV F protein is locked in its prefusion state, we focused on restraining the mobility of regions undergoing drastic conformational changes. These flexible areas were identified by calculating the root-mean-square-deviation (RMSD) of each $C\alpha$ atom in the prefusion conformation (R-1b protein, PDB: 7tn1) (32) compared to the postfusion structure (PDB: 3rrt) (51). Residue

positions displaying motion levels of at least 10Å were considered to be involved in the conformational switch and selected for disulfide scanning.

4.1.2 Structure preparation

Recognizing the dynamic nature of protein structures, we generated an ensemble of conformations for the R-1b protein to conduct a comprehensive exploration of new disulfide bonds. This methodology is especially pertinent for disulfide scanning since the identification of potential disulfides is significantly influenced by the distances between atoms. A total of 200 possible structures of the R-1b protein were produced by refining its crystal structure (PDB: 7tn1) with the Rosetta relax application (39–41). This refinement process was guided by electron density data to prevent substantial deviations from the initial protein configuration (65). The protein's density map was reconstructed from its map coefficients using the Phenix software version 1.15 (66) and the option "create map from map coefficients" (region padding= 0, and grid resolution factor= 0.3333). The relaxation process was carried out by assigning a weight of 35 to the density energy term of the Rosetta scoring function and performing five rounds of rotamer packing and minimization (39).

4.1.3 Design of disulfide bonds

For each conformation within the protein ensemble and every residue within the conformational switch area, we identified pairs of residues to be mutated to cysteine based on a $C\beta$-$C\beta$ distance ≤ 6Å. Subsequently, disulfide formation was enforced using the Rosetta Disulfidize mover and the PyRosetta interface (37, 38). Disulfides displaying rotation/translation distances "match_rt_limit" < 2 and disulfide scores "dslf_fa13" < 3.5 were selected for further refinement. This refinement was executed using the Rosetta FastRelax mover in RosettaScripts (39, 40, 67, 68). During the relaxation process, backbone energy minimization was permitted in segments of 10 residues up and downstream of the disulfide pair, while protein repacking was confined to a 10Å radius around the new bond. A total of five rounds of relaxation were conducted.

4.1.4 Selection of candidate disulfide bonds

To minimize significant disruption to the overall protein structure, disulfide designs were initially filtered based on a total RMSD value < 0.5Å compared to their parent configuration. Furthermore, we eliminated any non-native disulfides within a 7Å distance from native disulfides to prevent nonspecific interactions. Subsequently, to increase the likelihood of successful disulfide formation, we implemented a two-step filtering process to ensure the adequacy of the disulfide geometry. At first, we screened all predicted disulfides using the Rosetta disulfide geometry potential "dslf_fa13" with a threshold of < 0.1. Following this, we compared our disulfide bond angles (dihedrals $\chi1$, $\chi2$, $\chi3$, and angle $C\beta$-S-S) to a dataset of 300 high-resolution disulfide-containing structures (<1.5 Å) sourced from the Protein Data Bank. This dataset underwent prior relaxation using RosettaScripts and the FastRelax mover. Our disulfide candidates were then filtered based on their alignment with the observed angle ranges in these reference proteins.

In addition to evaluating the geometry, we ensured that newly introduced disulfides did not disrupt protein packing, especially when cysteine substitution involved buried hydrophobic residues. To achieve this, we identified buried hydrophobic residues in the monomeric parent structure using PyRosetta and considering a solvent-accessible surface area (SASA) $\leq$ 20Å^2 with a 2.2 Å probe size (69). Next, we assessed the packing quality within a 7Å radius around each buried residue using the PackstatCalculator (70) over five repetitions. This calculation was conducted both in the disulfide-containing model and the parent structure. Disulfide candidates were then considered when the packing quality was not disturbed by more than 0.2 units compared to the parent structure.

Finally, we incorporated the conformational dynamics of the RSV F protein to rank the potential prefusion-stabilization effect of the introduced disulfides. For this purpose, we utilized the root-mean-square deviation (RMSD) of the prefusion-to-postfusion transition as a quantitative metric to evaluate conformational dynamics. Our hypothesis suggests that regions with high RMSD are more likely to unfold first during the transition to the postfusion state. Therefore, disulfides hindering these initial rearrangements would be more effective at stabilizing the prefusion state. As a result, we ranked our disulfide candidates based on the highest RMSD observed within the residue pair forming the bond. This ranking was performed independently for the refolding region 1 and 2, as the conformational changes in the refolding region 2 depend on the earlier changes in refolding region 1 (30). The RMSD values were calculated using the same methodology employed for the identification of the conformational switch area.

4.2 Protein expression and characterization

4.2.1 Protein expression

Three R-1b disulfide-containing variants, namely SsA1 (V157C/N183C), SsA2 (A55C/L188C), and SsB1 (S443C/S466C), and the control R-1b, RSV A/A2 F (postfusion) (51), RSV A/A2 DS-Cav1 (7), and RSV B/18537 DS-Cav1 (52) constructs were expressed by transient transfection of FreeStyle 293-F cells (Thermo Fisher) with polyethylenimine (PEI) (Polysciences). All R-1b variants were produced in pCAGGS plasmids encoding the R-1b protein, a C-terminal T4 fibritin trimerization motif (Foldon), and a His6-tag. The sequence of the R-1b protein contained residues 1-105 and 137-513 with the respective substitutions under study, and a short linker replacing the furin cleavage site and the p27 peptide ("QARGSGSGR") (30). DNA sequences were codon optimized for human expression using the online tool GenSmart Codon Optimization (71). 293-F cells were incubated at 37°C and 8% CO_2 for three days after transfection, and proteins were purified by nickel affinity chromatography followed by size-exclusion chromatography (SEC). SEC was carried out using a Superdex200 column (Cytiva) and phosphate-buffered saline (PBS) buffer pH 7.4.

4.2.2 Thermal stability

Differential scanning fluorimetry (DSF) was used to monitor protein stability as a function of temperature. The samples analyzed contained 4μM of protein, 5X SYPRO orange fluorescent dye (Thermo Fisher), 5 mM MgCl$_2$, 50 mM KCl, and 50 mM Tris (pH 7.4). All measurements were performed by triplicates using a qPCR instrument (CFX Connect, BioRad) and a temperature gradient from 25 to 90°C with 0.5°C increments. The melting temperature of each protein was estimated based on the lowest point of the negative first derivative of the fluorescence signal.

4.2.3 Antigenic characterization

Antigenic preservation of prefusion epitopes was evaluated by bio-layer interferometry (BLI) using the prefusion-specific antibodies D25 (46, 47) (Thermo Fisher), hRSV90 (48), AM14 (47, 50) (Cambridge Biologics), and MPE8 (49). Binding against expressed designs was tested with 15 nM of the antibodies and eight concentrations of the antigens, starting from 200 nM and decreasing by two-fold dilutions. Prior to all binding assays, Protein A biosensors (GatorBio) were equilibrated for 20 min in BLI buffer (PBS buffer supplemented with 0.02% tween-20 (Promega) and 0.1% bovine serum albumin (BSA) (Sigma)). Subsequently, immobilization of the antibodies on the biosensor tips was allowed for 180s, followed by a baseline correction of 120s, and an association and dissociation steps of 180s each. All assays were performed on a GatorPrime BLI instrument (GatorBio) at a temperature of 30°C and frequency of 10 Hz. Binding constants were obtained with the GatorOne software 1.7.28, using a global association model 1:1 for D25, hRSV90, and MPE8, and 2:1 for AM14.

Antigenic preservation after heat treatment or exposure to various storage conditions was evaluated in the R1-b variant with the highest melting temperature (SsA1), along with the control proteins R1-b and RSV A/A2 DS-Cav1. For the heat treatment, the proteins were incubated for one hour at 65 and 70°C in a thermocycler with a heated lid (T100, BioRad). To evaluate storage conditions, the proteins were kept for one week at 25°C, one month at 5°C and -20°C, and over one year at -80°C. Subsequently, binding to D25, hRSV90, and MPE8 antibodies was measured following the protocol described above.

4.2.4 Disulfide bond detection through alkylation and mass spectrometry

Alkylation with iodoacetic acid (IAA) and iodoacetamide (IAM) was used to corroborate the formation of the disulfide bond V157C - N183C in the SsA1 protein. These alkylation reactions were intended to label free cysteines differentially from disulfide-bonding cysteines. Specifically, carboxymethyl groups were attached to free cysteines (IAA reaction), and carbamidomethyl groups were attached to disulfide-bonding cysteines (IAM reaction) after reduction of the disulfide bond. Following alkylation, the samples were digested, and peptides were analyzed through tandem liquid chromatography-mass spectrometry (LC-MS/MS).

The detailed steps of the process are described below:

- Alkylation reaction: 20 μL of SsA1 protein at 1.5 mg/mL were incubated for 30 minutes in the dark with 2 μL of 0.1M iodoacetic acid. The protein sample was denatured and

reduced by adding 0.5 µL of 0.5M dithiothreitol (DTT). The mixture was heated at 100°C for 5 minutes, and after cooling down, the reaction was allowed for 30 minutes at room temperature. The second alkylation was carried out by adding 2 µL of 0.5M iodoacetamide and incubating for 30 minutes.

- Deglycosylation: The alkylated sample was mixed with 100 µL of digest buffer (0.2% sodium deoxycholate (SDC) in 50 mM ammonium bicarbonate) and digested with 20U PNGase F (Lectenz Bio, Athens) in Sartorius Vivacon 500 (10K MWCO) for 2.5 hours at 37°C.

- Trypsin digestion: The sample in the filter was washed twice with 200 µL of 20 mM triethylammonium bicarbonate. 0.3 µg of Trypsin in 50 µL of 20 mM triethylammonium bicarbonate were added to the sample in the filter, and the digestion was carried out overnight at 37°C. The next day, the tryptic digests were spun out of the filter, and the remaining peptides in the filter were eluted with 100 µL of water. The tryptic peptides were dried by Vacufuge.

- LC-MS/MS: The mass spectrometry analyses were performed on a Thermo Fisher LTQ Orbitrap Elite Mass Spectrometer coupled with a Proxeon Easy NanoLC system (Waltham, MA) located at Proteomics and Mass Spectrometry Facility, University of Georgia. The enzymatic peptides were loaded into a reversed-phase column (self-packed column/emitter with Dr. Maisch ReproSil-pur C18AQ 120Å 3 µM resin) and directly eluted into the mass spectrometer. Briefly, the two-buffer gradient elution (0.1% formic acid as buffer A and 99.9% acetonitrile with 0.1% formic acid as buffer B) started with 0% buffer B for 2 minutes and then increased to 40% buffer B for 95 minutes and to 95% buffer B for 10 minutes. The MS data was obtained using the Xcalibur software (version 3.0, Thermo Fisher Scientific) and the data-dependent acquisition (DDA) method. A survey MS scan was acquired first, and then the top 10 ions in the MS scan were selected for following CID (collision-induced dissociation) and HCD (higher energy C trap dissociation) tandem mass spectrometry (MS/MS) analysis. Both MS and MS/MS scans were obtained by Orbitrap at the resolutions of 120,000 and 15,000, respectively. Protein identification and modification characterization were performed using Thermo Proteome Discoverer (version 3.0) with Mascot (Matrix Science) against Uniprot plus the SsA1 sequence and a modified contaminations database with commonly known contaminating proteins (Mascot).

4.3 Animal studies

4.3.1 Cotton rat immunization

Inbred 6-8 weeks-old *Sigmodon hispidus* female and male cotton rats (source: Sigmovir Biosystems, Inc., Rockville MD) were maintained and handled under veterinary supervision in accordance with the National Institutes of Health guidelines and Sigmovir Institutional Animal Care and Use Committee's approved animal study protocol (IACUC Protocol #15). Cotton rats were housed in clear polycarbonate cages and provided with standard rodent chow (Harlan #7004) and tap water *ad lib*. Groups of 5 or 6 animals (3 females/2 males or 3 females/3 males) were immunized intramuscularly with two different doses (10 µg or 100 µg) of either purified R-1b or SsA1 protein with AddaSO3 adjuvant (50% v/v) at weeks 0 and 4 (Prime and Boost) (Figure 4A). Control experiments were carried out by immunizing animals only with PBS (negative control), inoculating animals intranasally with 10^5 PFU of RSV A/A2 Live on week 0 (positive control for RSV A/A2 infection), or by immunizing animals with formalin-inactivated RSV (FI-RSV lot#100) diluted 1:100 in PBS (positive control for vaccine-enhanced disease). Bleeds were collected from the retro-orbital sinus at week 7 (Figure 4A), and sera were analyzed by ELISA, BLI, and neutralization assay.

4.3.2 RSV A/A2 challenge

RSV A/A2 (ATCC, Manassas, VA) was propagated in HEp-2 cells after serial plaque purification to reduce defective-interfering particles. A pool of virus designated as RSV/A2 Lot# 092215 SSM containing approximately 3.0×10^8 PFU/mL in sucrose stabilizing media was used for the *in vivo* experiment. Virus stock was stored at -80°C and had been characterized *in vivo* using the cotton rat model and validated for upper and lower respiratory tract replication. Vaccinated and control animals were inoculated intranasally at week seven with 0.1 mL of RSV/A2 (Lot# 092215 SSM) at 10^5 PFU per animal. Back titration on the challenge virus was performed to confirm the challenge dose. Cotton rats were euthanized on day five post-infection for analysis of viral load, lung histopathology, and mRNA gene expression.

4.3.3 RSV IgG measurement by ELISA

100 µL of purified R-1b (32), RSV A/A2 F (postfusion) (51), RSV A/A2 DS-Cav1 (7), and RSV B/18537 DS-Cav1 (52) at 2 µg/mL were coated onto 96 well ELISA plates (Immulon 2 HB, Thermo Fisher) at 4°C overnight. The next day, plates were washed with wash buffer (PBS buffer with 0.05% tween-20) and blocked with 200 µL/well of blocking buffer (wash buffer supplemented with 3% non-fat milk (LabScientific) and 0.5% BSA). After two hours of incubation at room temperature, plates were washed, and 100 µL/well of diluted serum from each rat was added and incubated for two hours at room temperature. Serum was serially diluted 1:3 in blocking buffer starting from a 1:20,000 or 1:60,000 (R1-b binding) dilution until a total of seven dilutions. Once the serum incubation finished, the plates were washed, and 100 µL/well of Rabbit anti-Cotton Rat IgG (1:1,000 in blocking buffer) (Invitrogen) was added and incubated for one hour at room temperature. The plates were washed again and 100 µL/well of Goat anti-Rabbit IgG-HRP (1:9,000 in blocking buffer) (Invitrogen) was added and incubated for one hour at room temperature. Finally, plates were washed and 100 µL/well of TMB substrate solution (Fisher Scientific) was added and incubated in the dark for 15 minutes. The reaction was stopped with 100 µL/well of 2M H_2SO_4 and the optical density (OD) was measured at 450 nm on a SpectraMax M2 Reader (Molecular Devices). All experiments were performed by duplicates and the averaged OD value was considered

for analysis. Serum titers were estimated with GraphPad Prism 9.0 (53) using the area under the curve (AUC) measurement with a baseline of 0.3 absorbance units and $\log_3$-transformed serum dilutions.

4.3.4 Antibody competition assays using BLI

Antibody binding competition against D25, hRSV90, MPE8, and 131-2A (54) (Millipore Sigma) was carried out to estimate epitope-specific responses after vaccination. Prior to data collection, anti-penta-His sensors (GatorBio) were hydrated for 20 minutes in BLI buffer (PBS buffer supplemented with 0.5% BSA and 0.05% tween-20, pH 7.4). The assay was initiated with an equilibration step in BLI buffer for 100s, followed by immobilization of the R-1b or RSV A2 F (postfusion) proteins at 20 µg/mL for 50s. The probes were then washed for 200s in blocking buffer (25% ChonBlock buffer (Chondrex Inc.) diluted in BLI buffer), and interaction with pooled serum samples (three weeks post-boost) was allowed for 700s. Sera were serially diluted 1:3 in blocking buffer, starting from a 1:10 dilution until a total of six dilutions. Blocking buffer with no serum and naïve serum from PBS-vaccinated rats (1:10 dilution) were also included as controls. After serum interaction, a baseline phase was carried out by dipping the probes in blocking buffer for 60s. Finally, the association of competing antibodies was performed for 700s. The MPE8 antibody was tested at 18 µg/mL, while the remaining antibodies were tested at 9 µg/mL. All antibodies were diluted in blocking buffer and the antigens were diluted in BLI buffer. The percentage of antibody competition was calculated as 1-(association response vaccinated serum/association response naïve serum) × 100%. Measurements were performed by duplicates and the averaged competition value was considered for analysis. All assays were performed with a GatorPrime BLI instrument at a temperature of 30°C and a frequency of 10 Hz.

4.3.5 RSV neutralizing antibody assay (60% reduction)

Heat-inactivated serum samples were diluted 1:20 with Eagle's Minimum Essential Medium (EMEM) and serially diluted further 1:4. Diluted serum samples were incubated with RSV A/A2 (25-50 PFU) for one hour at room temperature and inoculated in duplicates onto confluent HEp-2 monolayers in 24 well plates. After one hour of incubation at 37°C in a 5% CO2 incubator, the wells were overlayed with a 0.75% methylcellulose medium. After four days of incubation, the overlay was removed, and the cells were fixed with 0.1% crystal violet stain for one hour and then rinsed and air dried. The corresponding reciprocal neutralizing antibody titers were determined at the 60% reduction end-point of the virus control. The average value for two measurements was considered for analysis.

4.3.6 Lung and nose viral titration

Lung (en bloc and tri-sect, left section) and nasal tissue were homogenized in 3 mL of Hanks' Balanced Salt Solution (HBSS) supplemented with 10% Sucrose-Phosphate-Glutamate (SPG). Homogenates were clarified by centrifugation and diluted in EMEM. Confluent HEp-2 monolayers were infected in duplicates with diluted homogenates in 24 well plates. After one hour

incubation at 37°C in a 5% CO_2 incubator, the wells were overlaid with 0.75% methylcellulose medium. After 4 days of incubation, the overlay was removed, and the cells were fixed with 0.1% crystal violet stain for one hour and then rinsed and air dried. Plaques were counted and virus titer was expressed as plaque forming units per gram of tissue. The averaged value over two measurements was used for analysis.

4.3.7 Real-time PCR

Total RNA was extracted from homogenized tissue (lingular lobe) or cells using the RNeasy purification kit (QIAGEN). 1 µg of total RNA was used to prepare cDNA using Super Script II RT (Invitrogen) and oligo dT primer (1 µL, Invitrogen). For the real-time PCR reactions, the Bio-Rad iQ^{TM} SYBR Green Supermix was used in a final volume of 25 µL, with final primer concentrations of 0.5 µM. Reactions were set up in duplicates in 96-well trays. Amplifications were performed on a Bio-Rad iCycler for 1 cycle of 95°C for 3 min, followed by 40 cycles of 95°C for 10s, 60°C for 10s, and 72°C for 15s. The baseline cycles and cycle threshold (Ct) were calculated by the iQ5 software in the PCR Base Line Subtracted Curve Fit mode. Relative quantitation of DNA was applied to all samples. The standard curves were developed using a serially diluted cDNA sample most enriched in the transcript of interest (e.g., lungs from 6 hours post-RSV infection of FI-RSV-immunized animals). The Ct values were plotted against the $\log_{10}$ cDNA dilution factor, and these curves were used to convert the Ct values obtained for different samples to relative expression units. The averaged relative expression units for two measurements were then normalized to the level of β-actin mRNA ("housekeeping gene") expressed in the corresponding sample.

4.3.8 Pulmonary histopathology

The right section of the lungs was dissected and inflated with 10% neutral buffered formalin to their normal volume and then immersed in the same fixative solution. Following fixation, the lungs were embedded in paraffin, sectioned, and stained with hematoxylin and eosin (H&E). Four parameters of pulmonary inflammation were evaluated: peribronchiolitis (inflammatory cell infiltration around the bronchioles), perivasculitis (inflammatory cell infiltration around the small blood vessels), interstitial pneumonia (inflammatory cell infiltration and thickening of alveolar walls), and alveolitis (cells within the alveolar spaces). Slides were scored blind on a 0-4 severity scale. The scores were subsequently converted to a 0 -100% histopathology scale.

4.3.9 Statistical analysis

All statistical analyses were performed in R studio 4.1.0 using the tidyverse and rstatix packages. ELISA results and vaccine-enhanced disease assessment from R-1b and SsA1 vaccinations were compared by applying a two-tailed t-test. Neutralization and histopathology data were compared with the Mann-Whitney U test. The normality of each group was confirmed by a Shapiro wilk test, and the equality of variances was checked through Levene's test. The overall level of significance was set at 5%. Boxplot visualization was done with the seaborn package in Python 3.7.

Data availability statement

The original contributions presented in the study are included in the article/Supplementary Materials. Further inquiries can be directed to the corresponding author.

Ethics statement

The animal study was approved by Sigmovir Biosystems, Inc.'s Institutional Animal Care and Use Committee (IACUC). The study was conducted in accordance with the local legislation and institutional requirements.

Author contributions

KG: Writing – review & editing, Writing – original draft, Visualization, Validation, Software, Methodology, Investigation, Formal analysis, Data curation, Conceptualization. KY: Writing – review & editing, Validation, Methodology, Investigation, Formal analysis, Data curation. JB: Writing – review & editing, Validation, Methodology, Investigation, Formal analysis, Data curation. MB: Writing – review & editing, Validation, Resources, Methodology, Investigation, Formal analysis, Data curation. E-MS: Writing – review & editing, Writing – original draft, Visualization, Validation, Supervision, Software, Resources, Project administration, Methodology, Investigation, Funding acquisition, Formal analysis, Data curation, Conceptualization.

Funding

Acknowledgments

Conflict of interest

Authors KY, JB, and MB were employed by the company Sigmovir Biosystems, Inc. KG and E-MS are inventors of an ongoing US patent application No.18/404,463.

The author(s) declared that they were an editorial board member of Frontiers, at the time of submission. This had no impact on the peer review process and the final decision.

Publisher's note

All claims expressed in this article are solely those of the authors and do not necessarily represent those of their affiliated organizations, or those of the publisher, the editors and the reviewers. Any product that may be evaluated in this article, or claim that may be made by its manufacturer, is not guaranteed or endorsed by the publisher.

Supplementary material

The Supplementary Material for this article can be found online at: https://www.frontiersin.org/articles/10.3389/fimmu.2024.1406929/full#supplementary-material

References

1. Loomis RJ, Stewart-Jones GBE, Tsybovsky Y, Caringal RT, Morabito KM, McLellan JS, et al. Structure-based design of nipah virus vaccines: A generalizable approach to paramyxovirus immunogen development. *Front Immunol*. (2020) 11:1–16. doi: 10.3389/fimmu.2020.00842

2. Dang HV, Chan YP, Park YJ, Snijder J, Da Silva SC, Vu B, et al. An antibody against the F glycoprotein inhibits Nipah and Hendra virus infections. *Nat Struct Mol Biol*. (2019) 26:980–7. doi: 10.1038/s41594-019-0308-9

3. Stewart-Jones GBEE, Chuang GY, Xu K, Zhou T, Acharya P, Tsybovsky Y, et al. Structure-based design of a quadrivalent fusion glycoprotein vaccine for human parainfluenza virus types 1–4. *Proc Natl Acad Sci USA*. (2018) 115:12265–70. doi: 10.1073/pnas.1811980115

4. Wong SS, Webby RJ. Traditional and new influenza vaccines. *Clin Microbiol Rev*. (2013) 26:476–92. doi: 10.1128/CMR.00097-12

5. Hsieh C-L, Rush SA, Palomo C, Chou C-W, Pickens W, Más V, et al. Structure-based design of prefusion-stabilized human metapneumovirus fusion proteins. *Nat Commun*. (2022) 13:1–11. doi: 10.1038/s41467-022-28931-3

6. Ngwuta JO, Chen M, Modjarrad K, Joyce MG, Kanekiyo M, Kumar A, et al. Prefusion F-specific antibodies determine the magnitude of RSV neutralizing activity in human sera. *Sci Transl Med 7 309ra162*. (2015) 7:309ra162. doi: 10.1126/scitranslmed.aac4241

7. McLellan JS, Chen M, Joyce MG, Sastry M, Stewart-Jones GBE, Yang Y, et al. Structure-based design of a fusion glycoprotein vaccine for respiratory syncytial virus. *Science*. (2013) 342:592. doi: 10.1126/science.1243283

8. Crank MC, Ruckwardt TJ, Chen M, Morabito KM, Phung E, Costner PJ, et al. A proof of concept for structure-based vaccine design targeting RSV in humans. *Science*. (2019) 365:505–9. doi: 10.1126/science.aav9033

9. Harrison SC. Viral membrane fusion. *Nat Struct Mol Biol*. (2008) 15:690–8. doi: 10.1038/nsmb.1456

10. Graham BS. Vaccine development for respiratory syncytial virus. *Curr Opin Virol*. (2017) 23:107–12. doi: 10.1016/j.coviro.2017.03.012

11. Falloon J, Yu J, Esser MT, Villafana T, Yu L, Dubovsky F, et al. Postfusion F protein–based vaccine did not prevent respiratory syncytial virus illness in older adults. *J Infect Dis*. (2017) 216:1362–70. doi: 10.1093/infdis/jix503

12. Bullough PA, Hughson FM, Skehel JJ, Wiley DC. Structure of influenza haemagglutinin at the pH of membrane fusion. *Nature*. (1994) 371:37–43. doi: 10.1038/371037a0

13. Chen J, Lee KH, Steinhauer DA, Stevens DJ, Skehel JJ, Wiley DC. Structure of the hemagglutinin precursor cleavage site, a determinant of influenza pathogenicity and the origin of the labile conformation. *Cell*. (1998) 95:409–17. doi: 10.1016/S0092-8674(00)81771-7

14. Wilson IA, Skehel JJ, Wiley DC. Structure of the haemagglutinin membrane glycoprotein of influenza virus at 3 Å resolution. *Nature*. (1981) 289:366–73. doi: 10.1038/289366a0

15. Chen L, Gorman JJ, McKimm-Breschkin J, Lawrence LJ, Tulloch PA, Smith BJ, et al. The structure of the fusion glycoprotein of Newcastle disease virus suggests a novel paradigm for the molecular mechanism of membrane fusion. *Structure*. (2001) 9:255–66. doi: 10.1016/S0969-2126(01)00581-0

16. Swanson K, Wen X, Leser GP, Paterson RG, Lamb RA, Jardetzky TS. Structure of the Newcastle disease virus F protein in the post-fusion conformation. *Virology*. (2010) 402:372–9. doi: 10.1016/j.virol.2010.03.050

17. Yin HS, Paterson RG, Wen X, Lamb RA, Jardetzky TS. Structure of the uncleaved ectodomain of the paramyxovirus (hPIV3) fusion protein. *Proc Natl Acad Sci USA*. (2005) 102:9288–93. doi: 10.1073/PNAS.0503989102

18. Yin H-S, Wen X, Paterson RG, Lamb RA, Jardetzky TS. Structure of the parainfluenza virus 5 F protein in its metastable, prefusion conformation. *Nature*. (2006) 439:38–44. doi: 10.1038/nature04322

19. White JM, Delos SE, Brecher M, Schornberg K. Structures and mechanisms of viral membrane fusion proteins: Multiple variations on a common theme. *Crit Rev Biochem Mol Biol*. (2008) 43:189–219. doi: 10.1080/10409230802058320

20. Izaguirre G. The proteolytic regulation of virus cell entry by furin and other proprotein convertases. *Viruses*. (2019) 11:837. doi: 10.3390/v11090837

21. Skehel JJ, Bayley PM, Brown EB, Martin SR, Waterfield MD, White JM, et al. Changes in the conformation of influenza virus hemagglutinin at the pH optimum of virus mediated membrane fusion. *Proc Natl Acad Sci USA*. (1982) 79:968–72. doi: 10.1073/pnas.79.4.968

22. Chen J, Wharton SA, Weissenhorn W, Calder LJ, Hughson FM, Skehel JJ, et al. A soluble domain of the membrane-anchoring chain of influenza virus hemagglutinin (HA2) folds in Escherichia coli into the low-pH-induced conformation. *Proc Natl Acad Sci USA*. (1995) 92:12205–9. doi: 10.1073/pnas.92.26.12205

23. Eckert DM, Kim PS. Mechanisms of viral membrane fusion and its inhibition. *Annu Rev Biochem*. (2001) 70:777–810. doi: 10.1146/annurev.biochem.70.1.777

24. Earp LJ, Delos SE, Park HE, White JM. The many mechanisms of viral membrane fusion proteins. *Curr Top Microbiol Immunol*. (2004) 285:25–66. doi: 10.1007/3-540-26764-6_2

25. Jardetzky TS, Lamb RA. Activation of paramyxovirus membrane fusion and virus entry. *Curr Opin Virol*. (2014) 0:24. doi: 10.1016/j.coviro.2014.01.005

26. Joyce MG, Zhang B, Ou L, Chen M, Chuang GY, Druz A, et al. Iterative structure-based improvement of a fusion-glycoprotein vaccine against RSV. *Nat Struct Mol Biol*. (2016) 23:811–20. doi: 10.1038/nsmb.3267

27. Rutten L, Gilman MSA, Blokland S, Juraszek J, McLellan JS, Langedijk JPM. Structure-based design of prefusion-stabilized filovirus glycoprotein trimers. *Cell Rep*. (2020) 30:4540–4550.e3. doi: 10.1016/j.celrep.2020.03.025

28. Hsieh CL, Goldsmith JA, Schaub JM, DiVenere AM, Kuo HC, Javanmardi K, et al. Structure-based design of prefusion-stabilized SARS-CoV-2 Spikes. *Science*. (2020) 369:1501–5. doi: 10.1101/2020.05.30.125484

29. Wong JJW, Paterson RG, Lamb RA, Jardetzky TS. Structure and stabilization of the Hendra virus F glycoprotein in its prefusion form. *Proc Natl Acad Sci U. S. A.* (2016) 113:1056–61. doi: 10.1073/pnas.1523303113

30. Krarup A, Truan D, Furmanova-Hollenstein P, Bogaert L, Bouchier P, Bisschop IJMM, et al. A highly stable prefusion RSV F vaccine derived from structural analysis of the fusion mechanism. *Nat Commun*. (2015) 6:8143. doi: 10.1038/ncomms9143

31. Battles MB, Más V, Olmedillas E, Cano O, Vázquez M, Rodríguez L, et al. Structure and immunogenicity of pre-fusion-stabilized human metapneumovirus F glycoprotein. *Nat Commun*. (2017) 8:1–11. doi: 10.1038/s41467-017-01708-9

32. Gonzalez KJ, Huang J, Criado MF, Banerjee A, Tompkins S, Mousa JJ, et al. A general computational design strategy for stabilizing viral class I fusion proteins. *Nat Commun*. (2024) 15:1335. doi: 10.1038/s41467-024-45480-z

33. Craig DB, Dombkowski AA. Disulfide by Design 2.0: A web-based tool for disulfide engineering in proteins. *BMC Bioinf*. (2013) 14:0–6. doi: 10.1186/1471-2105-14-346

34. Salam NK, Adzhigirey M, Sherman W, Pearlman DA, Thirumalai D. Structure-based approach to the prediction of disulfide bonds in proteins. *Protein Eng. Des Sel*. (2014) 27:365–74. doi: 10.1093/protein/gzu017

35. Gao X, Dong X, Li X, Liu Z, Liu H. Prediction of disulfide bond engineering sites using a machine learning method. *Sci Rep*. (2020) 10:1–9. doi: 10.1038/s41598-020-67230-z

36. Le QAT, Joo JC, Yoo YJ, Kim YH. Development of thermostable Candida Antarctica lipase B through novel in silico design of disulfide bridge. *Biotechnol Bioeng*. (2012) 109:867–76. doi: 10.1002/bit.24371

37. Chaudhury S, Lyskov S, Gray JJ. PyRosetta: a script-based interface for implementing molecular modeling algorithms using Rosetta. *Bioinformatics*. (2010) 26:689. doi: 10.1093/bioinformatics/btq007

38. Bhardwaj G, Mulligan VK, Bahl CD, Gilmore JM, Harvey PJ, Cheneval O, et al. Accurate *de novo* design of hyperstable constrained peptides. *Nature*. (2016) 538:329–35. doi: 10.1038/nature19791

39. Tyka MD, Keedy DA, André I, Dimaio F, Song Y, Richardson DC, et al. Alternate states of proteins revealed by detailed energy landscape mapping. *J Mol Biol*. (2011) 405:607–18. doi: 10.1016/j.jmb.2010.11.008

40. Khatib F, Cooper S, Tyka MD, Xu K, Makedon I, Popović Z, et al. Algorithm discovery by protein folding game players. *Proc Natl Acad Sci USA*. (2011) 108:18949–53. doi: 10.1073/pnas.1115898108

41. Conway P, Tyka MD, DiMaio F, Konerding DE, Baker D. Relaxation of backbone bond geometry improves protein energy landscape modeling. *Protein Sci*. (2014) 23:47–55. doi: 10.1002/pro.2389

42. Alford RF, Leaver-Fay A, Jeliazkov JR, O'Meara MJ, DiMaio FP, Park H, et al. The rosetta all-atom energy function for macromolecular modeling and design. *J Chem Theory Comput*. (2017) 13:3031–48. doi: 10.1021/acs.jctc.7b00125

43. O'Meara MJ, Leaver-Fay A, Tyka MD, Stein A, Houlihan K, Dimaio F, et al. Combined covalent-electrostatic model of hydrogen bonding improves structure prediction with Rosetta. *J Chem Theory Comput*. (2015) 11:609–22. doi: 10.1021/ct500864r

44. Zhang L, Durr E, Galli JD, Cosmi S, Cejas PJ, Luo B, et al. Design and characterization of a fusion glycoprotein vaccine for Respiratory Syncytial Virus with improved stability. *Vaccine*. (2018) 36:8119–30. doi: 10.1016/j.vaccine.2018.10.032

45. Che Y, Gribenko AV, Song X, Handke LD, Efferen KS, Tompkins K, et al. Rational design of a highly immunogenic prefusion-stabilized F glycoprotein antigen for a respiratory syncytial virus vaccine. *Sci Transl Med*. (2023) 15:eade6422. doi: 10.1126/scitranslmed.ade6422

46. McLellan JS, Chen M, Leung S, Graepel KW, Du X, Yang Y, et al. Structure of RSV fusion glycoprotein trimer bound to a prefusion-specific neutralizing antibody. *Science*. (2013) 340:1113–7. doi: 10.1126/SCIENCE.1234914

47. Kwakkenbos MJ, Diehl SA, Yasuda E, Bakker AQ, Van Geelen CMM, Lukens MV, et al. Generation of stable monoclonal antibody-producing B cell receptor-positive human memory B cells by genetic programming. *Nat Med*. (2010) 16:123–8. doi: 10.1038/nm.2071

48. Mousa JJ, Kose N, Matta P, Gilchuk P, Crowe JE. A novel pre-fusion conformation-specific neutralizing epitope on the respiratory syncytial virus fusion protein. *Nat Microbiol*. (2017) 2:16271. doi: 10.1038/nmicrobiol.2016.271

49. Corti D, Bianchi S, Vanzetta F, Minola A, Perez L, Agatic G, et al. Cross-neutralization of four paramyxoviruses by a human monoclonal antibody. *Nature*. (2013) 501:439–43. doi: 10.1038/nature12442

50. Gilman MSAA, Moin SM, Mas V, Chen M, Patel NK, Kramer K, et al. Characterization of a prefusion-specific antibody that recognizes a quaternary, cleavage-dependent epitope on the RSV fusion glycoprotein. *PLoS Pathog*. (2015) 11:1–17. doi: 10.1371/journal.ppat.1005035

51. Mclellan JS, Yang Y, Graham BS, Kwong PD. Structure of respiratory syncytial virus fusion glycoprotein in the postfusion conformation reveals preservation of neutralizing epitopes. *J Virol*. (2011) 85:7788–96. doi: 10.1128/JVI.00555-11

52. Joyce MG, Bao A, Chen M, Georgiev IS, Ou L, Bylund T, et al. Crystal structure and immunogenicity of the ds-cav1-stabilized fusion glycoprotein from respiratory syncytial virus subtype b authors. *Pathog Immun*. (2019) 4:294–323. doi: 10.20411/pai.v4i2

53. Chen B, Cheng Y, Calder L, Harrison SC, Reinherz EL, Skehel JJ, et al. A Chimeric Protein of Simian Immunodeficiency Virus Envelope Glycoprotein gp140 and Escherichia coli Aspartate Transcarbamoylase. *J Virol*. (2004) 78:4508–16. doi: 10.1128/JVI.78.9.4508-4516.2004

54. Anderson LJ, Bingham P, Hierholzer JC. Neutralization of respiratory syncytial virus by individual and mixtures of F and G protein monoclonal antibodies. *J Virol*. (1988) 62:4232. doi: 10.1128/jvi.62.11.4232-4238.1988

55. Rossey I, McLellan JS, Saelens X, Schepens B. Clinical potential of prefusion RSV F-specific antibodies. *Trends Microbiol*. (2018) 26:209–19. doi: 10.1016/j.tim.2017.09.009

56. Baden LR, El Sahly HM, Essink B, Kotloff K, Frey S, Novak R, et al. Efficacy and safety of the mRNA-1273 SARS-CoV-2 vaccine. *N Engl J Med*. (2021) 384:403–16. doi: 10.1056/NEJMoa2035389

57. Du L, He Y, Zhou Y, Liu S, Zheng BJ, Jiang S. The spike protein of SARS-CoV - A target for vaccine and therapeutic development. *Nat Rev Microbiol*. (2009) 7:226–36. doi: 10.1038/nrmicro2090

58. Chang LA, Phung E, Crank MC, Morabito KM, Villafana T, Dubovsky F, et al. A prefusion-stabilized RSV F subunit vaccine elicits B cell responses with greater breadth and potency than a postfusion F vaccine. *Sci Transl Med*. (2022) 14:1–12. doi: 10.1126/scitranslmed.ade0424

59. Tian D, Battles MB, Moin SM, Chen M, Modjarrad K, Kumar A, et al. Structural basis of respiratory syncytial virus subtype-dependent neutralization by an antibody targeting the fusion glycoprotein. *Nat Commun*. (2017) 8:1–7. doi: 10.1038/s41467-017-01858-w

60. Battles MB, Langedijk JP, Furmanova-Hollenstein P, Chaiwatpongsakorn S, Costello HM, Kwanten L, et al. Molecular mechanism of respiratory syncytial virus fusion inhibitors. *Nat Chem Biol*. (2016) 12:87–93. doi: 10.1038/nchembio.1982

61. Roymans D, Alnajjar SS, Battles MB, Sitthicharoenchai P, Furmanova-Hollenstein P, Rigaux P, et al. Therapeutic efficacy of a respiratory syncytial virus fusion inhibitor. *Nat Commun*. (2017) 8:167. doi: 10.1038/s41467-017-00170-x

62. Yan D, Lee S, Thakkar VD, Luo M, Moore ML, Plemper RK. Cross-resistance mechanism of respiratory syncytial virus against structurally diverse entry inhibitors. *Proc Natl Acad Sci USA*. (2014) 111:E3441–E3449. doi: 10.1073/pnas.1405198111

63. Byrne PO, Blade EG, Fisher BE, Ambrozak DR, Ramamohan AR, Graham BS, et al. Prefusion stabilization of the Hendra and Langya virus F proteins. *J Virol*. (2024) 98:e01372–23. doi: 10.1128/jvi.01372-23

64. Stewart-Jones GBEE, Thomas PV, Chen M, Druz A, Joyce MG, Kong WP, et al. A cysteine zipper stabilizes a pre-fusion F glycoprotein vaccine for respiratory syncytial virus. *PLoS One*. (2015) 10:e0128779. doi: 10.1371/journal.pone.0128779

65. Wang RYR, Song Y, Barad BA, Cheng Y, Fraser JS, DiMaio F. Automated structure refinement of macromolecular assemblies from cryo-EM maps using Rosetta. *Elife*. (2016) 5:e17219. doi: 10.7554/eLife.17219

66. Adams PD, Afonine PV, Bunkóczi G, Chen VB, Davis IW, Echols N, et al. PHENIX: a comprehensive Python-based system for macromolecular structure solution. (2010) 66:213–21. doi: 10.1107/S0907444909052925

67. Maguire JB, Haddox HK, Strickland D, Halabiya SF, Coventry B, Griffin JR, et al. Perturbing the energy landscape for improved packing during computational protein design. *Proteins Struct Funct Bioinforma*. (2020) 89:1–14. doi: 10.22541/au.158986804.41133682

68. Fleishman SJ, Leaver-Fay A, Corn JE, Strauch EM, Khare SD, Koga N, et al. Rosettascripts: A scripting language interface to the Rosetta Macromolecular modeling suite. *PLoS One*. (2011) 6:e20161. doi: 10.1371/journal.pone.0020161

69. Durham E, Dorr B, Woetzel N, Staritzbichler R, Meiler J. Solvent accessible surface area approximations for rapid and accurate protein structure prediction. *J Mol Model*. (2009) 15:1093–108. doi: 10.1007/s00894-009-0454-9

70. Sheffler W, Baker D. osettaHoles: Rapid assessment of protein core packing for structure prediction, refinement, design, and validation. *Protein Sci*. (2009) 18:229–239. doi: 10.1002/pro.8

71. Fang L. Codon optimization. *International Patent WO2020024917A1* (2020).